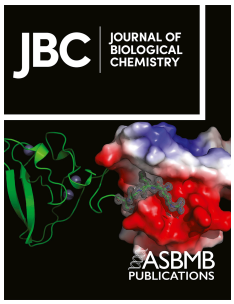

A conserved allosteric element controls specificity and activity of functionally divergent PP2C phosphatases from *B. subtilis*

Kristin Ho, Niels Bradshaw

PII: S0021-9258(21)00295-7

DOI: https://doi.org/10.1016/j.jbc.2021.100518

Reference: JBC 100518

To appear in: *Journal of Biological Chemistry*

Received Date: 10 December 2020

Revised Date: 1 March 2021

Accepted Date: 4 March 2021

Please cite this article as: Ho K, Bradshaw N, A conserved allosteric element controls specificity and activity of functionally divergent PP2C phosphatases from *B. subtilis*, *Journal of Biological Chemistry* (2021), doi: https://doi.org/10.1016/j.jbc.2021.100518.

A conserved allosteric element controls specificity and activity of functionally divergent PP2C phosphatases from *B. subtilis*

Kristin Ho[1] and Niels Bradshaw[1*]

[1]Department of Biochemistry, Brandeis University, Waltham, USA

* corresponding author; niels@brandeis.edu

Running title: Control of phosphatase activity and specificity

Keywords: Allosteric regulation, Bacillus, protein phosphatase 2C (PP2C), stress response, substrate specificity, bacterial transcription, bacterial protein phosphatase, bacterial signal transduction, cell signaling, metal ion-protein interaction

Abstract

Reversible phosphorylation relies on highly regulated kinases and phosphatases that target specific substrates to control diverse cellular processes. Here, we address how protein phosphatase activity is directed to the correct substrate under the correct conditions. The serine/threonine phosphatase SpoIIE from *Bacillus subtilis*, a member of the widespread protein phosphatase 2C (PP2C) family of phosphatases, is activated by movement of a conserved α-helical element in the phosphatase domain to create the binding site for metal-cofactor. We hypothesized that this conformational switch could provide a general mechanism for control of diverse PP2C phosphatases. The *B. subtilis* phosphatase RsbU responds to different signals, acts

on a different substrate, and produces a more graded response than SpoIIE. Using an unbiased genetic screen, we isolated mutants in the α-helical switch region of RsbU that are constitutively active, indicating conservation of the switch mechanism. Using phosphatase activity assays with phosphoprotein substrates, we found that both phosphatases integrate substrate recognition with activating signals to control metal-cofactor binding and substrate dephosphorylation. This integrated control provides a mechanism for PP2C phosphatases to produce specific responses by acting on the correct substrates, under the appropriate conditions.

Introduction

Protein kinases and phosphatases regulate diverse biological processes by controlling the phosphorylation state of target proteins, requiring that they select specific substrates and act on them at the correct time and place. Protein kinases have conserved allosteric elements that control kinase activity in response to regulatory inputs and have deep active site grooves that facilitate recognition of cognate substrates (1-3). While all protein kinases belong to a single superfamily of related enzymes, protein phosphatases come from multiple evolutionarily unrelated lineages (4). Determining how each family of phosphatases achieves regulation and specificity will reveal mechanistic differences that distinguish each phosphatase family and may suggest specific strategies for targeting phosphatases with small molecules.

We focus here on the PP2C family of serine/threonine phosphatases, members of which are found across all kingdoms of life (5, 6). PP2C phosphatases are precisely regulated to control a diverse range of processes including stress response, development, virulence, and cell growth and death in all kingdoms of life, but their mechanisms of regulation and substrate specificity are unknown (4, 7). To address this question, we developed a system to compare substrate selection

and regulation of two PP2C phosphatases, SpoIIE and RsbU, which co-exist in the same bacterial cell, but respond to different signals and act on distinct phospho-protein substrates.

SpoIIE controls the developmental program of spore development in the bacterium *B. subtilis* (Figure 1A) (8). Following asymmetric cell division, SpoIIE is stabilized against proteolysis and is activated by multimerization in small cells (9). The multimerization, stabilization, and activation of SpoIIE is mediated by its unique regulatory domain. Upon activation, SpoIIE dephosphorylates SpoIIAA to activate a cell-specific transcription factor (σ^F) (Figure 1A) (8, 10). We recently found that SpoIIE is activated by rotation of an α-helical element at the base of the phosphatase domain to form the binding site for the catalytically essential metal ions (we refer to the metal ions as "metal-cofactor" and use Mn^{2+} as the metal for all experiments in this study, Figure 1B) (11). The regulatory α-helical element we described is a conserved feature of the PP2C phosphatase domain, and we hypothesized that it is preserved as a regulatory switch for phosphatases in this family (11).

The phosphatase RsbU has a PP2C phosphatase domain that is related to SpoIIE (17% sequence identity, 40% similarity, and includes a region predicted to form the α-helical switch) (SF1A and SF1B) but has an unrelated N-terminal regulatory domain (Figure 1A and SF1A) and responds to different signals to initiate the general stress response in *B. subtilis* (Figure 1A) (12). The general stress response describes a broad transcriptional response that is activated by diverse bacterial species in response to changing conditions and coordinates processes including virulence, antibiotic resistance, and biofilm formation (13). A common mechanism for activation of a general stress response relies on a PP2C phosphatase that recognizes the initiating signal. This appears to be the most evolutionarily ancient and broadly conserved function of PP2C phosphatases across the bacterial kingdom. To activate the general stress response under

conditions of environmental stress in *B. subtilis*, RsbU binds to an activating protein (RsbT) and dephosphorylates RsbV. RsbV then activates the transcription factor σ^B, which controls the general stress response transcriptional program in *B. subtilis* (Figure 1A) (12). It is essential that SpoIIE and RsbU act with high fidelity on their cognate substrates (14); aberrant dephosporylation of RsbV-P and activation of the general stress response during sporulation blocks spore development (15) and dephosphorylation of SpoIIAA-P in non-sporulating cells is toxic.

In addition to sensing different signals and acting on different substrates, SpoIIE and RsbU exhibit different response profiles. Whereas SpoIIE initiates a switch-like developmental transition, RsbU initiates a graded response with amplitudes scaled to the strength of the initiating signal (16, 17). These phosphatase-substrate pairs thus provide an experimentally tractable system within a well-characterized model organism with which to identify principles for how PP2C family phosphatases are regulated and achieve substrate specificity.

Using a combined forward-genetic and biochemical approach to probe the regulation and specificity of RsbU and SpoIIE, we found that the regulatory switch is a conserved element that ensures each phosphatase is only active at the correct time, under the correct conditions, and when in complex with the correct substrate protein.

Results

SpoIIE principally achieves specificity by stabilizing the transition state

To assess how SpoIIE achieves specificity for its cognate substrate SpoIIAA as opposed to its non-cognate substrate RsbV, we used the C-terminal phosphatase domain in isolation ($SpoIIE^{590-827}$) (Figure 1B). We selected this construct to test the hypothesis that specificity can

be encoded by the PP2C catalytic domain alone and to identify potentially conserved mechanisms of specificity. At least three steps of the phosphatase reaction could in principle contribute to specificity: substrate recognition, chemistry, and metal-cofactor binding. To isolate the contributions of substrate recognition and chemistry we held the metal-cofactor constant at saturating levels (10 mM $MnCl_2$). Under these conditions, $SpoIIE^{590-827}$ was specific, dephosphorylating SpoIIAA-P approximately 3,500-fold more efficiently than the off-pathway substrate, RsbV-P (SpoIIAA-P k_{cat}/K_M = 0.68±0.04 $min^{-1}\mu M^{-1}$, RsbV-P k_{cat}/K_M = 0.00020±.00002 $min^{-1}\mu M^{-1}$) (Figure 1C). This specificity was principally the result of an increased k_{cat} for the cognate substrate (18.7±0.4 min^{-1} for SpoIIAA, 0.064±0.005 min^{-1} for RsbV) but was enhanced by a lower K_M for the cognate substrate (20±1 µM for SpoIIAA, 255±39 µM for RsbV) (Figure 1D). Thus, specificity is achieved by directing 3.4 kcal/mol of the specific binding energy for the cognate substrate to stabilizing the transition state and 1.5 kcal/mol to stabilization of the enzyme substrate complex (Fig 1E). Here we discuss K_M as representing "substrate recognition", but also note that the lack of a lag-phase in pre-steady-state reactions, the µM K_M values for substrate, and minute timescale k_{cat} are all suggestive of the K_M being equal to the K_D of the enzyme-substrate complex.

The regulatory switch couples substrate recognition to metal-cofactor binding

The conserved regulatory switch moves to activate SpoIIE by recruiting metal-cofactor to the active site (Figure 1B). We hypothesized that substrate binding is favored when the switch is in the active conformation, coupling substrate binding to metal-cofactor binding. To investigate this hypothesis, we took advantage of a gain-of-function mutant of SpoIIE (valine 697 to alanine, V697A) in which substitution of a single amino acid in the hydrophobic core of the phosphatase

domain biases the switch to the active state (Figure 1B) (11, 18, 19). The V697A substitution decreased the specificity of SpoIIE, increasing the k_{cat}/K_M for RsbV-P 150-fold compared to a 5-fold increase for SpoIIAA-P (Figure 2A). In the experiments described below, we analyzed the effect of the V697A substitution on K_M, k_{cat}, and metal-cofactor binding with both the cognate and non-cognate substrates.

Substrate recognition (K_M): The V697A substitution decreased the K_M of SpoIIE$^{590-827}$ for both SpoIIAA-P (10-fold) and RsbV-P (5-fold) (Figure 2A), suggesting that substrate binding is favored when SpoIIE is in the active conformation.

Chemistry (k_{cat}): The V697A substitution increased the maximal catalytic rate (k_{cat}) of SpoIIE$^{590-827}$ for the non-cognate substrate nearly forty-fold while having a modest effect on the cognate substrate (Figure 2A). Thus, the switch controls the maximum catalytic rate of SpoIIE in addition to controlling metal-cofactor binding. Furthermore, the conformational flexibility of the switch can differentially affect the catalytic rate for cognate and non-cognate substrates.

Metal-cofactor binding: To monitor metal-cofactor recruitment, we held the substrate concentration constant and measured SpoIIE activity with varied concentrations of $MnCl_2$ (Figure 2B). Consistent with our previous observations, the V697A substitution decreased the concentration of $MnCl_2$ required for SpoIIE$^{590-827}$ to dephosphorylate SpoIIAA-P ($K_{1/2}$ 3.1±0.9 mM for WT SpoIIE$^{590-827}$ and $K_{1/2}$ 0.16±0.05 mM for SpoIIE$^{590-827}$ V697A). In contrast, the V697A substitution increases the $MnCl_2$ concentration required for dephosphorylation for the non-cognate substrate RsbV-P ($K_{1/2}$ of 2.0±0.4 mM for WT SpoIIE$^{590-827}$and $K_{1/2}$ of 19±2 mM for SpoIIE$^{590-827}$ V697A). Cooperativity of metal-cofactor binding (Hill coefficient of two, inset panels Figure 2B), yields a switch-like response profile, appropriate for initiation of a developmental transition.

Together, these kinetic parameters demonstrate that the switch mediates coupling between metal-cofactor binding, substrate recognition, and chemistry and that the V697A substitution shifts binding energy for the non-cognate substrate from metal-cofactor binding to chemistry, reducing specificity at saturating metal-cofactor concentrations (summarized in Figure 2C).

The SpoIIE regulatory domain controls metal-cofactor binding, substrate recognition and chemistry.

PP2C phosphatases have regulatory domains that control their activity (4, 11). We therefore repeated the above analysis with the phosphatase domain of SpoIIE together with a portion of the regulatory domain (SpoIIE$^{457-827}$). We chose this fragment because it is a well-behaved soluble protein whose crystal structure we previously reported (11) (Figure 3A). Although the regulatory domain is truncated, this fragment allowed us to test how contact with an accessory domain affects the behavior of the switch. Similar to our observations with SpoIIE$^{590-827}$, SpoIIE$^{457-827}$ was specific for SpoIIAA-P (SpoIIAA-P k_{cat}/K_M = 0.039±0.002 $min^{-1}\mu M^{-1}$, RsbV-P k_{cat}/K_M = 7.2±0.2 x10^{-5} $min^{-1}\mu M^{-1}$) (Figure 3A) and its specificity for its cognate substrate was reduced by the V697A substitution (k_{cat}/K_M for RsbV-P increases 100-fold, but was unaffected for SpoIIAA-P) (Figure 3A).

SpoIIE$^{457-827}$ exhibited several notable differences from the phosphatase domain alone (SpoIIE$^{590-827}$). First, the regulatory domain increased the K_M of SpoIIE for both cognate and non-cognate substrates, such that the concentration dependence of phosphatase activity was linear even at concentrations of substrate above 100 µM (Figure 3A). Second, the regulatory domain altered how the V697A substitution affected metal-cofactor binding; whereas the

substitution decreased the concentration of $MnCl_2$ required for $SpoIIE^{457-827}$ to dephosphorylate SpoIIAA-P (Figure 2A), it had no effect on the concentration of $MnCl_2$ required to dephosphorylate RsbV-P (Figure 3B).

Together, these findings (summarized in Figure 3C) are consistent with coupling between substrate recognition, chemistry, and metal-cofactor recruitment and indicate that regulatory domains can influence all three steps through the switch.

A role for the switch-element in activating RsbU phosphatase activity

Next, we addressed whether coupled activation, substrate recognition, and metal-cofactor binding through the switch is conserved for the stress-response phosphatase, RsbU (Figure 1A). First, we tested the hypothesis that the switch mediates RsbT activation of RsbU. We took an unbiased approach to interrogate the mechanism of RsbU activation by performing a genetic screen to isolate variants of RsbU that are active in the absence of RsbT. We reasoned that if the switch is important for RsbU regulation, we would isolate activating mutations in the switch region. We generated a library of randomly mutagenized *rsbU* variants and induced their expression in a strain harboring a LacZ reporter for σ^B activity and selected for variants that activated σ^B. From this screen, we identified two amino acid substitutions in the RsbU phosphatase domain, both at M166 (M166L, and M166V), that activated σ^B in the absence of RsbT as visualized by *lacZ* dependent color change on X-Gal plates (Figure 4A shows plates with $rsbU^{M116L/V}$ introduced at the native locus; Figure SF2A shows the plates with strains expressing $rsbU^{M166L/V}$ using the plasmid based system used in the screen). Activation of σ^B was dependent on expression of the mutagenized RsbU because both pathways known to dephosphorylate RsbV-P were deleted from the parental strain (and all other strains described

below), and activation in plasmid-based systems depended on induction of RsbU expression (Figure SF2A). M166 is in the N-terminal α-helix of the switch and is predicted to pack in the hydrophobic core of the phosphatase domain (Figure 4B). The position of these mutations is reminiscent of the activating mutation V697A in SpoIIE (Figure 4B) and the position of M166 in the RsbU switch provides independent evidence that the switch is required for RsbU activation.

Our analysis of the SpoIIE V697A mutation revealed that it acts by biasing the switch towards the active conformation, allowing for partial activation in the absence of signal, and potentiating the response to low levels of signal (11). Consistent with a similar mechanism for the M166 mutations, we observed that when the plasmids used to isolate the *rsbU*$^{M166L/V}$ variants were introduced to strains with *rsbT*, σ^B activity was elevated compared to Δ*rsbT* strains on plates (SF2A). A similar phenomenon was not qualitatively apparent on plates for cells expressing *rsbU*$^{M116L/V}$ at the native locus (Figure 4A). However, we observed that the σ^B activity of liquid-grown cells expressing *rsbU*^{M116L} sharply increased between OD_{600} 0.5-1.0 and peaked as the cells entered stationary phase (OD_{600} 1.5) (Figure 4C, top panel). This cell-density dependent effect was potentiated by RsbT; σ^B activity was ten-fold lower in strains that lacked *rsbT (*Figure 4C, bottom panel). A similar cell-density dependent increase in σ^B activity was not detected in cells expressing wild-type *rsbU* regardless of the presence of *rsbT (*Figure 4C, top panel). These data suggest that mutation of M166 sensitizes RsbU to activation by RsbT – even at levels that are normally insufficient to elicit a response.

The *rsbU*^{M166L} mutation also potentiated the RsbT-mediated response to environmental stress. Cells with *rsbU*^{M166L} integrated at the native chromosomal locus had an elevated response to a well-characterized environmental stressor (4% ethanol by volume) that activates RsbU through RsbT (12). Stress was introduced at low ODs (0.1-0.2) to minimize the impact of cell

density on σ^B activity in *rsbU*^{M166L} expressing cells. The elevated response of cells expressing *rsbU*^{M166L} mirrored the characteristic dynamics of the sharp and transient increase in σ^B activity of wild-type cells followed by a gradual ramp-down of activity (Figure 4D and SF2B, top panel) (. As this response depends on both RsbT and RsbU, strains lacking either of these genes failed to respond to the stressor (Figure 4D, bottom panel). Together, the position of M166 in the RsbU regulatory switch and its impact on RsbU activity implicate the switch as a conserved element to control phosphatase activity in response to cellular signals.

Mechanisms of regulation and specificity are conserved between SpoIIE and RsbU

If the switch-element acts similarly to activate SpoIIE and RsbU, a simple prediction is that activation of RsbU by RsbT would decrease the concentration of metal-cofactor required for activity. We reconstituted RsbU activation by RsbT and found that RsbT decreased the $K_{1/2}$ of RsbU for Mn^{2+} by nearly 100-fold ($K_{1/2}$ 1.0±0.1 mM in the presence of RsbT and 77±9 mM in the absence of RsbT) (Figure 5A). In contrast to SpoIIE, RsbU activity towards its cognate substrate was non-cooperative with respect to Mn^{2+} concentration (Figure 5A right panels). Whereas SpoIIE regulates a developmental transition, for which an all-or-nothing response is important, RsbU regulates a stress response, for which the graded response that non-cooperative activation affords may be advantageous.

In our *in vitro* assays, RsbT additionally enhanced the maximal catalytic activity of RsbU towards RsbV-P 10-fold (k_{cat} 25±2 min^{-1} in the presence of RsbT and 0.44±0.06 min^{-1} in the absence of RsbT) (Figure 5A), consistent with previous observations (12, 20). This suggests that, as we observed for SpoIIE, control of chemistry and metal-cofactor binding are coupled,

providing nearly a 1000-fold increase in the activity of RsbU at concentrations of metal ion below the $K_{1/2}$ (as would be expected in the cytoplasm) (21, 22).

Reconstitution of RsbU activation by RsbT further allowed us to determine how specificity is maintained upon phosphatase activation. Like SpoIIE, RsbU is specific: RsbU had higher catalytic activity towards its cognate substrate (k_{cat} 0.44±0.06 min^{-1} for RsbV-P and 0.0012±0.0004 min^{-1} for SpoIIAA-P), and bound both cognate and non-cognate substrates tightly (K_M 0.9 µM for SpoIIAA-P and 1.5 µM for RsbV-P; K_M values were difficult to determine accurately because of limitations of detection for substrate proteins) (Figure 5B).

As with the cognate substrate, RsbT enhanced RsbU catalytic activity towards SpoIIAA-P (a 300-fold increase to k_{cat} 0.32±0.02 min^{-1}) (Figure 5B). However, RsbT did not substantially change the affinity of metal-cofactor binding with the non-cognate substrate (K_M 8±3 mM in the absence of RsbT and 20±6 mM in the presence of RsbT), similar to the V697A mutation of $SpoIIE^{457-827}$ (Figure 5A). We did note partial cooperativity for manganese with SpoIIAA as the substrate (Hill coefficient of 1.4±0.1 without RsbT and 1.6±0.3 with RsbT). This mild effect is consistent with our observation that the substrate influences the binding of metal in the active site. RsbT also had little impact on SpoIIAA-P binding (approximate K_M 1 µM in the absence of RsbT and 0.3 µM in the presence of RsbT) (Figure 5B). Thus, specificity is maintained because RsbT activation fails to stimulate metal-cofactor binding for RsbU in the presence of its non-cognate substrate (summarized in Figure 5C).

Conclusions

By examining two phosphatases, we found that PP2C regulation and specificity is mediated by a conserved allosteric element that is functionally flexible to respond to varied

signals and to discriminate between substrate proteins. This regulatory mechanism is orchestrated by an allosteric switch that integrates activating signals and binding to cognate substrate to control metal-cofactor binding in the active site and catalytic activity. This coupling of regulatory inputs, chemistry, and substrate recognition provides a unified mechanism to control diverse signaling pathways.

By what mechanism could the PP2C switch-element transduce regulatory inputs to coordinate substrate recognition, metal-cofactor binding, and chemistry? In a parsimonious model, both regulatory domains and substrates might directly contact and influence the conformation of the switch. This is supported by our findings that a fragment of the regulatory domain of SpoIIE shifts the energetic balance between substrate recognition, chemistry, and metal-cofactor recruitment. Furthermore, the switch is the structural feature of SpoIIE that mediates these changes in phosphatase activity and substrate recognition. The switch is situated directly below the active site, where it would likely contact substrate proteins and might also control the maximum catalytic rate by precise positioning of the phosphoserine bond and the metal-cofactors in the active site. Such an architecture is present in the single available structure of a PP2C phosphatase bound to its substrate protein (the phosphatase Hab1 bound to SnRK2). SnRK2 makes direct contacts with the Hab1 switch and to a variable region (termed “the flap”) that packs against the switch (23).

Dimerization may also be a widespread regulatory mechanism for PP2C phosphatases. SpoIIE is activated by formation of a dimer in which the switch elements of the two phosphatase domains make direct contacts and lock the switch element in the active state (11). One attractive possibility is that the specific contacts between the switch elements in the phosphatase dimer are conserved. This is supported by the fact that similar contacts have been observed in dimeric

structures of *P. aeruginosa* phosphatases RssB and SiaA (24-25). Dimerization also plays an important role in RsbU activation; a fragment of the RsbU regulatory domain crystallized as a dimer and a groove formed at the dimer interface was shown to be critical for RsbT binding to RsbU (20). However, the mechanism of how RsbU dimerization is coupled to phosphatase activation is unknown.

We hypothesize that this conserved allosteric switch may regulate diverse PP2C phosphatases across the tree of life. Regulatory domains from diverse PP2C phosphatases also pack against the switch, suggesting that coupling between substrate recognition, metal-cofactor binding, and activity could be broadly conserved (11, 26-28). Additionally, structural analysis and molecular dynamics simulations of human PP2Cα revealed a network of interactions that link the switch element, metal binding in the active site, and the flap subdomain (29). Hydrogen-deuterium exchange experiments revealed increased mobility of the switch helices (α1 and α2) at sub-saturating metal-cofactor concentrations and when the binding site for a third metal ion was disrupted by mutation of its coordinating residue, D146 (29). Further highlighting the similarities between the bacterial and human phosphatases, SpoIIE V697 and PP2Cα D146 both sit at the end of β-strand 6, two amino acids away from each other in a sequence alignment. These data suggest that the structural features of the PP2C catalytic domain that we identify as controlling phosphatase activity and specificity are broadly conserved.

The mechanism we describe here for PP2C phosphatase regulation and specificity, however, is qualitatively different from what is known about evolutionarily unrelated serine/threonine phosphatases from other families. For both the PPP phosphatases (including PP1, PP2A, and calcineurin) and FCP/CTD phosphatases, the catalytic domain itself is thought to be relatively promiscuous for substrates. Substrate specificity is instead imposed by diverse

regulatory subunits that tether substrates in proximity of the catalytic center, control subcellular localization of the phosphatase, and/or gate substrate access to the active site (4).

Because phosphatases control signaling pathways that contribute to multiple disease processes, they are attractive drug targets, but their lack of deep and thus classically druggable active site pockets has made development of small molecule modulators difficult (30). Recent successes, however, have targeted phosphatase regulatory mechanisms: PP2A inhibitors that target the conformation of regulatory subunits (31), PP2A activators that promote the assembly of specific regulatory subunits into holoenymes (32), and allosteric modulators of active site gating for the protein tyrosine phosphatase, SHP2 (33). The allosteric regulatory mechanism of PP2C phosphatases may also similarly provide strategies for the development of modulators. Indeed, allosteric inhibitors of the oncogenic PP2C phosphatase Wip1 were identified that bind to the flap subregion, although the mechanism of action of these inhibitors is unknown (34, 35). We propose that these and future PP2C modulators may act on the allosteric switch we here describe as coordinating substrate recognition, chemistry, and metal-cofactor binding.

Materials and Methods

Growth conditions.

Liquid cultures were grown in Lennox lysogeny broth (LB) while colonies were grown on LB containing Bacto agar. The antibiotics used were MLS (50 µg/ml erythromycin, 250 µg/ml lincomycin), chloramphenicol (20 µg/ml for *E. coli*), carbenicillin (100 µg/ml), and kanamycin (10 µg/ml for *B. subtilis* or 50 µg/ml for *E. coli*). When indicated, 80 µg/ml of 5-bromo-4-chloro-3-indolyl-β-D-galactopyranoside (X-gal) and 1 mM Isopropyl β-d-1-thiogalactopyranoside (IPTG) were added to growth medium to visualize σ^B reporter activity on plates.

Protein expression constructs

SpoIIAA and SpoIIAB were expressed in BL21 (DE3) Rosetta2 pLysS cells as 6H-sumo fusions in pET23a made by ligation of the coding sequence in pET23a 6H-sumo digested with NotI/AgeI (. SpoIIAA-P was produced in BL21 (DE3) cells containing pET-YSBLIC 6H-3C-spoIIAA–spoIIAB as reported (36). SpoIIE$^{590-827}$, SpoIIE$^{457-827}$, RsbT, RsbU, RsbV, and RsbW were produced with 3C cleavable 6H tags in BL21 (DE3) cells (constructs were made by insertion of the coding sequence to pET47b vectors digested with XmaI/XhoI by isothermal assembly). Mutations were introduced to SpoIIE expression constructs using QuikChange site directed mutagenesis. RsbV-P was produced by co-expressing RsbV and RsbW using a pET47b vector generated by isolation of the coding sequences for RsbV and RsbW from genomic DNA, yielding a construct with RsbV fused to a 3C cleavable 6H tag followed by untagged RsbW. All strains used are listed in the table of strains.

Protein expression and purification

Proteins were expressed and purified using slight modifications to previous methods (11). All proteins were purified to greater than 95% purity as assessed by Coomassie stained SDS-PAGE gel. Unless otherwise noted, protein expression was induced with 1 mM IPTG for 14-18 hours at 14ºC in BL21 (DE3) cells that had been grown in LB to OD_{600} of 0.6 at room temperature. Details for purification of individual proteins follows:

SpoIIE (same protocol for all variants) was purified from cell pellets lysed (using a microfluidizer) in 50 mM K•HEPES pH 8.0, 200 mM NaCl, 10% glycerol (v/v), 0.5 mM DTT, 20 mM imidazole, 0.1 mg/ml PMSF. Lysates were clarified by spinning for 30 min at 16,000 RPM in a Sorvall SS-34 rotor at 4℃. Protein was bound to a HisTrap HP column on an AKTA FPLC, was washed, and then was eluted with a gradient to 200 mM imidazole. The 6H tag was cleaved overnight in dialysis with PreScission protease, and the tag and protease were removed by flowing over Ni-NTA resin. SpoIIE was next purified on a Resource Q column equilibrated in 50 mM HEPES pH 8.0, 100 mM NaCl, 2 mM EDTA, 2 mM DTT and eluted with a gradient to 500 mM NaCl. The SpoIIE containing fractions were spin concentrated and gel-filtered on a 120 ml Superdex 75 column equilibrated in 20 mM K•HEPES pH 8.0, 100 mM NaCl, 10% glycerol (v/v), 2 mM DTT. Protein was spin-concentrated to approximately 400 µM and flash-frozen and stored at –80ºC.

SpoIIAA was expressed for 4 hours at 37ºC. Cell pellets were resuspended in 20 mM K•HEPES pH 7.5, 200 mM NaCl, 0.5 mM DTT, 0.1 mg/ml PMSF (5 ml/l of culture). Cells were lysed using a cell disruptor in one-shot mode (Constant Systems, Daventry, United Kingdom) and lysates were clarified by spinning for 30 min at 16,000 RPM in a Sorvall SS-34 rotor at 4℃. Protein was bound to Ni-NTA resin (1 ml/l of culture) on column by gravity flow, washed with

buffer containing 20 mM imidazole, and eluted with 200 mM imidazole. The 6H-sumo tag was cleaved using 10µl of a 100 µM stock of ULP1 in overnight dialysis at 16ºC to 20 mM K•HEPES pH 7.5, 200 mM NaCl, 10% glycerol (v/v), 0. 5 mM DTT. The 6H-sumo tag was subtracted by flowing over Ni-NTA resin equilibrated in the cleavage and dialysis buffer. The cleaved protein was then spin-concentrated and gel-filtered on a 120ml Superdex 75 column equilibrated in 50 mM K•HEPES pH 8.0, 100 mM NaCl, 10% glycerol (v/v), 2 mM DTT. Protein was concentrated to approximately 400 µM, flash-frozen and stored at -80ºC.

SpoIIAB was expressed for 4 hours at 37ºC. Cell pellets were resuspended in 50 mM K•HEPES pH 7.5, 200 mM NaCl, 10 mM $MgCl_2$, 0.5% Triton X-100 (v/v), 0.5 mM DTT, 0.1 mg/ml PMSF (5ml/l of culture). Cells were lysed using a cell disruptor in one-shot mode (Constant Systems, Daventry, United Kingdom) and lysates were clarified by spinning for 30 min at 16,000 RPM in a Sorvall SS-34 rotor at 4℃. Protein was bound to Ni-NTA resin (1 ml/l of culture) on column by gravity flow, washed with buffer containing 20 mM imidazole, and eluted with 200 mM imidazole. The 6H-sumo tag was left un-cleaved to aid in removal from phosphorylation reactions. SpoIIAB was spin-concentrated and gel-filtered on a 120 ml Superdex 75 column equilibrated in 50 mM K•HEPES pH 7.5, 175 mM NaCl, 10 mM $MgCl_2$, 10% glycerol (v/v), 2 mM DTT. Protein was concentrated to approximately 400 µM, supplemented to 50% glycerol (v/v) and flash-frozen and stored at -80ºC.

SpoIIAA-P was purified from cells co-expressing 6H-3C-SpoIIAA and untagged SpoIIAB for 4 hours at 37ºC. Cell pellets were resuspended in 20 mM K•HEPES pH 7.5, 200 mM NaCl, 0.5 mM DTT, 0.1 mg/ml PMSF (5 ml/l of culture). Cells were lysed using a cell disruptor in one-shot mode (Constant Systems, Daventry, United Kingdom) and lysates were clarified by spinning for 30 min at 16,000 RPM in a Sorvall SS-34 rotor at 4℃. Protein was

bound to a HisTrap HP column on an AKTA FPLC, was washed with buffer containing 20 mM imidazole and 500 mM NaCl, and eluted with a gradient to 300 mM imidazole. The tag was cleaved using PreScission protease overnight dialysis at 4ºC. The cleaved protein was then spin-concentrated and gel-filtered on a 120 ml Superdex 75 column equilibrated in 50 mM K•HEPES pH 8.0, 100 mM NaCl, 10% glycerol (v/v), 2 mM DTT. Protein was concentrated to approximately 400 µM, flash-frozen and stored at –80ºC.

SpoIIAB was expressed for 4 hours at 37ºC. Cell pellets were resuspended in 50 mM K•HEPES pH 7.5, 200 mM NaCl, 10 mM $MgCl_2$, 0.5% Triton X-100 (v/v), 0.5 mM DTT, 0.1 mg/ml PMSF (5ml/l of culture). Cells were lysed using a cell disruptor in one-shot mode (Constant Systems, Daventry, United Kingdom) and lysates were clarified by spinning for 30 min at 16,000 RPM in a Sorvall SS-34 rotor at 4℃. Protein was bound to Ni-NTA resin (1 ml/l of culture) on column by gravity flow, washed with buffer containing 20 mM imidazole, and eluted with 200 mM imidazole. The 6H-sumo tag was left un-cleaved to aid in removal from phosphorylation reactions. SpoIIAB was spin-concentrated and gel-filtered on a 120 ml Superdex 75 column equilibrated in 50 mM K•HEPES pH 7.5, 175 mM NaCl, 10 mM $MgCl_2$, 10% glycerol (v/v), 2mM DTT. Protein was concentrated to approximately 400 µM, supplemented to 50% glycerol (v/v) and flash-frozen and stored at –80ºC.

RsbT was purified from cell pellets lysed (using a microfluidizer) in 20 mM K•HEPES pH 7.5, 200 mM NaCl, 10% glycerol (v/v), 0.5 mM DTT, 20 mM imidazole, 0.1 mg/ml PMSF. Lysates were clarified by spinning for 30 min at 16,000 RPM in a Sorvall SS-34 rotor at 4℃. Protein was bound to Ni-NTA resin (1 ml/l of culture) on column by gravity flow, washed, and eluted with 200 mM imidazole. The 6H tag was cleaved overnight in dialysis with PreScission protease, and the tag and protease were removed by flowing over Ni-NTA resin. RsbT was spin

concentrated and gel-filtered on a 120 ml Superdex 75 column equilibrated in 20 mM K•HEPES pH 7.5, 150 mM NaCl, 10% glycerol (v/v), 2 mM DTT. Protein was spin-concentrated to approximately 40 µM (additional concentration led to aggregation) and was flash-frozen and stored at –80ºC.

RsbU was purified from cell pellets lysed (using a microfluidizer) in 50 mM K•HEPES pH 8.0, 200 mM NaCl, 10% glycerol (v/v), 0.5 mM DTT, 20 mM imidazole, 0.1 mg/ml PMSF. Lysates were clarified by spinning for 30 min at 16,000 RPM in a Sorvall SS-34 rotor at 4℃. Protein was bound to a HisTrap HP column on an AKTA FPLC, was washed, and then was eluted with a gradient to 200 mM imidazole. The 6H tag was cleaved overnight in dialysis with PreScission protease, and the tag and protease were removed by flowing over Ni-NTA resin. Cleaved RsbU was spin concentrated and gel-filtered on a 120 ml Superdex 75 column equilibrated in 20 mM K•HEPES pH 8.0, 100 mM NaCl, 10% glycerol (v/v), 2 mM DTT. The RsbU containing fractions were then purified on a Resource Q column equilibrated in 50 mM HEPES pH8.0, 100 mM NaCl, 2 mM EDTA, 2 mM DTT and eluted with a gradient to 500 mM NaCl. This final step removes a degradation product present in some RsbU preparations. Protein was supplemented with 10% glycerol (v/v), spin-concentrated to approximately 400 µM and flash-frozen and stored at –80ºC.

RsbV was purified from cell pellets lysed (using a microfluidizer) in 20 mM K•HEPES pH 7.5, 200 mM NaCl, 10% glycerol (v/v), 0.5 mM DTT, 20 mM imidazole, 0.1 mg/ml PMSF. Lysates were clarified by spinning for 30 min at 16,000 RPM in a Sorvall SS-34 rotor at 4℃. Protein was bound to Ni-NTA resin (1 ml/l of culture) on column by gravity flow, washed, and eluted with 200 mM imidazole. The 6H tag was cleaved overnight in dialysis with PreScission protease, and the tag and protease were removed by flowing over Ni-NTA resin. RsbT was spin

concentrated and gel-filtered on a 120 ml Superdex 75 column equilibrated in 20 mM K•HEPES pH 7.5, 150 mM NaCl, 10% glycerol (v/v), 2 mM DTT. Protein was spin-concentrated to approximately 400 µM and flash-frozen and stored at –80ºC.

RsbW was purified from cell pellets lysed (using a microfluidizer) in 20 mM K•HEPES pH 7.5, 10 mM $MgCl_2$, 200 mM NaCl, 10% glycerol (v/v), 0.5 mM DTT, 20 mM imidazole, 0.1 mg/ml PMSF. Lysates were clarified by spinning for 30 min at 16,000 RPM in a Sorvall SS-34 rotor at 4℃. Protein was bound to a HisTrap HP column on an AKTA FPLC, washed, and eluted with a gradient to 250 mM imidazole. The 6H tag was left un-cleaved to aid removal after phosphorylation reactions. RsbW was then purified on a Resource Q column equilibrated in 50 mM HEPES pH 7.5, 200 mM NaCl, 10 mM $MgCl_2$, 2 mM DTT and eluted with a gradient to 1M NaCl. RsbW containing fractions were spin concentrated and gel-filtered on a 120 ml Superdex 75 column equilibrated in 50 mM K•HEPES pH 7.5, 150 mM NaCl, 10% glycerol (v/v), 2 mM DTT. Protein was spin-concentrated to approximately 100 µM and flash-frozen and stored at –80ºC.

RsbV-P was purified from cells co-expressing 6H-3C-RsbV and untagged RsbW that were grown at 37ºC and induced with 1 mM IPTG for 4 hours at 37ºC. Cells were lysed (using a microfluidizer) in 50 mM K•HEPES pH 7.5, 50 mM KCl, 10% glycerol (v/v), 0.5 mM DTT, 20 mM imidazole, 0.1 mg/ml PMSF. Lysates were clarified by spinning for 30 min at 16,000 RPM in a Sorvall SS-34 rotor at 4℃. Protein was bound to a HisTrap HP column on an AKTA FPLC, washed, and eluted with a gradient to 250 mM imidazole. RsbVW containing fractions were then gel-filtered using a 120 ml Superdex 75 column and fractions containing either RsbV or RsbVW complex were collected. The sample was supplemented with 5 mM ATP, 10 mM $MgCl_2$, and PreScission protease and placed in dialysis in 200 ml of buffer also supplemented with $MgCl_2$

and ATP at room temperature overnight. The 6H tag and protease were removed by flowing over Ni-NTA resin and the protein was gel-filtered again on a Superdex 75 column equilibrated in 50 mM K•HEPES pH 8.0, 100 mM NaCl, 2 mM DTT, 10% glycerol (v/v). Free RsbV-P was collected and complete phosphorylation was confirmed by isoelectric focusing. Protein was spin-concentrated to approximately 400 µM and flash-frozen and stored at –80ºC.

Phosphatase Assays

Phosphatase assays were performed using methods reported previously (9) with modifications as described. To produce ^{32}P-labeled SpoIIAA-P, 75 µM SpoIIAA, 5 µM SpoIIAB and 50 µCi of γ-^{32}P ATP were incubated overnight at room temperature in 50 mM K•HEPES pH 7.5, 50 mM KCl, 750 µM $MgCl_2$, 2 mM DTT. Unincorporated nucleotide was removed from the reaction mixture by buffer exchange using a Zeba spin column (Pierce) equilibrated in 20 mM K•HEPES pH 7.5, 200 mM NaCl, 2 mM DTT. The sample was then flowed over Q-sepharose resin to remove SpoIIAB. SpoIIAA-P was then buffer exchanged to the buffer used for subsequent assays using a Zeba spin column equilibrated in 50 mM K•HEPES pH 8.0, 100 mM NaCl. Labeled SpoIIAA-P was aliquoted and frozen at –80ºC for future use.

To produce ^{32}P labeled RsbV-P, 50 µM RsbV, 5 µM RsbW and 200 µCiof γ-^{32}P ATP were incubated overnight at room temperature in 50 mM K•HEPES pH 7.5, 50 mM KCl, 10 mM $MgCl_2$, 2 mM DTT. Unincorporated nucleotide was removed from the reaction mixture by buffer exchange using a Zeba spin column (Pierce) equilibrated in 50 mM K•HEPES pH 8.0, 100 mM NaCl, 20 mM imidazole. 6H-tagged RsbW was then removed by binding to Ni-NTA resin. The flowthrough containing RsbV-P was then exchanged to the buffer used for subsequent assays using two successive Zeba spin columns equilibrated in 50 mM K•HEPES pH 8.0, 100 mM

NaCl to remove all unincorporated nucleotide and free phosphate. Labeled RsbV-P was aliquoted and frozen at –80ºC for future use.

All phosphatase assays were performed at room temperature in 25 mM K•HEPES pH 8, 100 mM NaCl, 100 µg/ml BSA (to prevent protein sticking to tubes). The concentrations of enzyme, substrate, and $MnCl_2$ were varied as indicated. 10 µM RsbT was additionally added to reactions as indicated. We note that the magnitude of effects reported for RsbT are lower limits because higher concentrations of RsbT could not be tested due to aggregation of RsbT at high concentration. Reactions were stopped in 0.5 M EDTA pH 8.0, 2% Triton X-100 (v/v) and run on PEI-Cellulose TLC plates developed in 1 M $LiCl_2$, 0.8 M Acetic Acid, and imaged on a Typhoon (GE Life Sciences). Phosphatase assays were performed more than three independent times as separate experiments.

Strain construction

B. subtilis strains were constructed using standard molecular genetic techniques (in the PY79 strain background (and were validated to contain the correct constructs by double-crossover recombination at the correct insertion site. All strains are used in this study are described in table of strains. A σ^B reporter strain (KC479 (14)) was used as a parent strain for all *B. subtilis* strains. A parent strain (Δ*rsbPQ* Δ*rsbTU rsbV-FLAG amyE::ctc-lacZ*) was generated for the screen of *rsbT*-independent *rsbU* variants. To generate a marked deletion of *rsbPQ*, the genomic regions 500 bp upstream and downstream of *rsbPQ* were amplified and ligated to a kanamycin resistance cassette using standard SOE PCR techniques. The linear DNA fragment was inserted into KC479 using standard techniques. Transformants were selected based on kanamycin resistance and confirmed by colony PCR and sequencing. A clean deletion of *rsbTU* was generated by

generating a gBlock (IDT DNA Technologies) of regions corresponding to 500 bp upstream of *rsbT* and 500 bp downstream of *rsbU* ligated together. This fragment was introduced into the HindIII and EcoRI sites of pminiMAD2 (40). Standard genetic techniques were used to excise the chromosomal copy of *rsbTU*. Mutants were confirmed by colony PCR and sequencing of the genomic region. Similarly, a clean deletions of *sigB, rsbT,* and *rsbU* were generated, with the modification that we utilized a gBlock (IDT DNA Technologies) of regions corresponding to 500 bp upstream and 500 bp downstream of the appropriate genes. A single FLAG tag was introduced at the C-terminus of *rsbV* using the pminiMAD2 vector. Point mutations of the *rsbU* gene were similarly introduced using the pminiMAD2 vector and confirmed by colony PCR and sequencing.

An inducible expression vector (pKH001-Pspank-*rsbU*) was generated to screen for *rsbT*-independent variants of *rsbU.* A gBlock (IDT DNA Technologies) was generated containing a super-folding *gfp* gene flanked by AgeI and NotI sites and introduced into plasmid pDR110 (at the HindIII and SphI sites using standard genetic techniques. The fragment of the resulting plasmid containing the *lacI* gene and the inducible *sfgfp* gene were PCR amplified and inserted into vector pHB201 (42) at the SacI and KpnI sites using standard genetic techniques to generate pKH001-Pspank-*sfgfp*. To generate expression constructs for *rsbU* and *rsbTU,* the appropriate genes were PCR amplified from genomic DNA from PY79 using a high-fidelity polymerase and introduced at the AgeI and NotI sites using isothermal assembly.

To generate libraries of pKH001-Pspank-*rsbU* containing mutagenized *rsbU,* the *rsbU* gene was PCR amplified from genomic DNA from PY79 using error-prone PCR, utilizing the natural error rate of Taq polymerase. Mutagenized *rsbU* was introduced at the AgeI and NotI sites using

standard genetic techniques. Plasmids were introduced into the parent strain (Δ*rsbPQ* Δ*rsbTU rsbV-FLAG amyE::ctc-lacZ*) using standard *B. subtilis* transformation techniques.

Screen

Six independent pools of mutagenized *rsbU* were generated by amplifying *rsbU* under mutagenic PCR conditions using GoTaq polymerase (Promega) and an additional 2mM $MgCl_2$. These pools of mutagenized *rsbU* were sub-cloned into linearized plasmid using isothermal assembly to generate pKH001-P (spank)-*rsbU* and transformed separately into *E. coli* DH5α cells to propagate plasmids. Mutation rate was confirmed to be approximately one single nucleotide polymorphism (SNP) per one kilobase of DNA by sequencing selected clones. *E. coli* colonies were pooled to generate mixed populations of mutagenized pKH001-Pspank-*rsbU*, and this DNA was introduced separately into independent clones of the parent strain. Cultures were grown in selective media and plated on selective medium containing IPTG and X-gal for 2 days at 37C. Approximately 12,000 mutant strains were analyzed. Blue colonies were selected and phenotypes were confirmed by re-streaking on indicator medium before plasmids were miniprepped and sequenced. Mutation M166V was isolated independently in four out of six pools of mutagenized *rsbU* and M166L was isolated once. Mutations were re-introduced into pKH001-Pspank-*rsbU* through QuikChange PCR and introduced into fresh parent backgrounds to confirm that phenotypes were dependent on expression of mutated *rsbU*.

Liquid based beta-galactosidase assays

Beta-galactosidase assays to measure σ^B -reporter activity were adapted from previously described protocols (37)**.** In brief, cells were grown to desired OD, spun down, and frozen at -

80ºC. Thawed pellets were resuspended in Z-buffer (60 mM Na_2HPO_4 $7H_20$, 40 mM NaH_2PO_4 H_20, 10 mM KCl, 1mM $MgSO_4$, 50 mM 2-mercaptoethanol) and kept on ice. Cells were arrayed in a 96 well plate and the OD_{600} was measured to assess cell culture density. Cells were lysed in Z-buffer containing a final concentration of 10 mg/ml lysozyme for 30 minutes at 37ºC. *o*-nitrophenyl-β-D-galactoside (ONPG) was dissolved in Z-buffer (4mg/ml) and added to lysed cells to a final concentration of 0.67 mg/ml. Absorbance at 420 nm (to measure ONPG cleavage) and 550 nm (to control for light scattering caused by cell debris) was measured over 40 minutes and the rate of LacZ production was calculated from the slope of the linear phase of $A_{420} - 1.75*A_{550}$ (between 300-1500 seconds). Miller units were calculated using the formula that 1 Miller Unit = $1000* (A_{420} – (1.75*A_{550}))/ (t*v*OD_{600})$; t is time in minutes, and v is the volume of the reaction in milliliters.

Figure Preparation:

Figures from structural models were generated using PyMol (43) and UCSF Chimera (44). The sequence alignment in supporting figure SF1 was constructed and validated using UCSF Chimera and rendered using Geneious R7.

Data Availability:

All data is contained within the manuscript or available to be shared upon request (please contact corresponding author).

Supporting Information:

This article contains supporting information (supporting figures SF1 and SF2 and supporting tables S1-S3).

Acknowledgements:

Richard Losick has been extremely helpful in writing this manuscript and launching the Bradshaw lab. The authors also thank Chris Miller, Lizbeth Hedstrom, Dorothee Kern, Rachelle Gaudet, Julia Kardon, and members of the Bradshaw lab for discussions and for critical reading of the manuscript.

Author Contributions:

NB and KH designed the experiments, performed experiments, analyzed the data, prepared figures, and wrote the manuscript.

Funding and additional information

Funding for this work was from startup funds from Brandeis University to Niels Bradshaw, and NIH grant GM18568 to Richard Losick.

Competing Interests:

The authors have no competing interests.

Figure 1. SpoIIE discriminates between cognate and non-cognate substrates. a. The pathways controlling activity of the transcription factors σ^F and σ^B are diagrammed. The phosphatases SpoIIE (IIE) and RsbU dephosphorylate paralogous substrate proteins SpoIIAA-P (AA-P) and RsbV-P (V-P). The activity of RsbU is dependent upon activation by RsbT. In the unphosphorylated state, SpoIIAA and RsbV bind to anti-sigma-factor proteins SpoIIAB (AB) and RsbW (W), displacing and activating the sigma factors. **b.** Domain diagrams of SpoIIE and RsbU. The N-terminal regulatory regions of these proteins are unique, while the PP2C domains share 17% identity. The regulatory region of SpoIIE contains an N-terminal degradation tag (black) followed by 10 transmembrane domains (gray) (aa 49-320). Both SpoIIE (magenta) (aa 320-589) and RsbU (blue) (aa) contain unrelated regulatory domains. The PP2C domain of SpoIIE (aa 590-827) has been crystallized (11), and contains an α-helical regulatory switch (orange), which coordinates the binding of metal-cofactor along with metal binding residues D795, D746, and D628 (red) through the positioning the backbone carbonyl of G629. The PP2C domain of RsbU (aa 121-335) has not been crystallized, but is predicted to contain a similar α-helical regulatory switch. The metal binding residues show conservation between the two proteins (the detailed alignment can be seen in Figure SF1). **c.** Structures of SpoIIE in the inactive (top left, PDBID 5MQH) and active (top right, PDBID 5UCG) states. The α-helical switch is represented in orange and the sidechains that coordinate divalent cations in the active site are shown as sticks. Manganese ions are modeled in the active site of SpoIIE from the structure of metal bound RsbX and are represented as spheres. Valine 697 is shown as green spheres. Below each structure is a cartoon representation of the active site as it is controlled by the switch. In the inactive state, residue V697, shown in green, is modeled to be in a hydrophobic

pocket, while in the active site it is exposed to a hydrophilic patch. **d.** SpoIIE$^{590\text{-}827}$ phosphatase activity with SpoIIAA-P (red) or RsbV-P (blue) as substrate. Reactions with SpoIIAA-P as substrate were performed as multiple turnover reactions with 0.1 µM SpoIIE$^{590\text{-}827}$ and varying concentrations of SpoIIAA-P. Reactions with RsbV-P were performed as single turnover reactions (due to the extremely slow rates of reaction), using trace concentrations of RsbV-P with varying concentrations of SpoIIE$^{590\text{-}827}$. All reactions contained 10 mM $MnCl_2$. Data are fit to the linear equation observed rate = (k_{cat}/K_M)*[SpoIIAA-P or SpoIIE] and are plotted on log/log axes. e**.** Plots of the data from C including higher concentrations of SpoIIAA-P and SpoIIE. Data are fit using nonlinear curve fitting (Kaleidagraph) to the equation observed rate = k_{cat}*[SpoIIAA-P or SpoIIE]/ (K_M+ [SpoIIAA-P or SpoIIE]). f**.** A reaction coordinate diagram summarizing the data from d and e.

Figure 2. SpoIIE specificity is controlled by the switch. a. Plots showing the dephosphorylation of SpoIIAA-P (red) or RsbV-P (blue). The bar plot (left) summarizes the impact of the V697A substitution on the k_{cat}/K_M of SpoIIE$^{590\text{-}827}$. Data from SpoIIE^{V697A} are displayed in light colors. Reactions with SpoIIAA-P as substrate were performed as multiple-turnover reactions with varying concentrations of SpoIIAA-P and 0.04µM SpoIIE$^{590\text{-}827\ V697A}$ (the reduced K_M for this variant and SpoIIAA-P necessitated a lower concentration than used for SpoIIE$^{590\text{-}827}$). Slow reactions with RsbV-P were performed as single-turnover reactions (necessary due to slow rates of reaction), using trace concentrations of RsbV-P with varying concentrations of SpoIIE$^{590\text{-}827\ V697A}$. Data for wt SpoIIE are from the same experiment as shown in Figure 1D. All reactions contained 10 mM $MnCl_2$. To calculate k_{cat}/K_M, data from concentrations below the K_M are fit to the linear equation observed rate = (k_{cat}/K_M)*[SpoIIAA-P

or SpoIIE]. Error bars are the error of the fit. Right is a plot of the data, but including higher concentrations of SpoIIAA-P and SpoIIE. Data are fit using nonlinear curve fitting (Kaleidagraph) to the equation observed rate = k_{cat}*[SpoIIAA-P or SpoIIE]/ (K_M+ [SpoIIAA-P or SpoIIE]). **b.** SpoIIE activity as a function of $MnCl_2$ concentration, with SpoIIAA-P (red) or RsbV-P (blue). Multiple turnover reactions with SpoIIAA-P as substrate included 0.1 µM SpoIIE and 50 µM SpoIIAA-P. Single turnover reactions with RsbV-P as substrate included 50 µM SpoIIE and trace RsbV-P. Data are fit to a cooperative model using the equation k_{obs} = k_{cat}*$[MnCl_2]^2$/ ($K_{1/2}$+ $[MnCl_2]^2$). Hill plots from the data are shown to the right and are fit to a linear equation. For $SpoIIE^{590-827}$ with SpoIIAA-P *h* is 2.0 (1.7 for V697A) and 1.7 with RsbV-P (1.8 for V697A). **c.** A summary of kinetic parameters in the reaction scheme for dephosphorylation by SpoIIE. S indicates the phosphoprotein substrate and P indicates the product.

Figure 3. SpoIIE activity and specificity is influenced by the regulatory domain. a. Plots showing the dephosphorylation of SpoIIAA-P (red) and RsbV-P by a fragment of SpoIIE ($SpoIIE^{457-827}$) that includes part of the regulatory domain. The fragment of the regulatory domain is diagramed above in blue with the phosphatase domain gray and the switch in orange. Data from $SpoIIE^{457-827\ V697A}$ are displayed in light colors. The k_{cat}/K_M values displayed in the bar plot are derived from the data displayed in the right graph with concentrations below the K_M fit to the linear equation observed rate = (k_{cat}/K_M)*[SpoIIAA-P or SpoIIE]. Error bars are the error of the fit. Data in the right plot were fit using nonlinear curve fitting (Kaleidagraph) to the equation observed rate = k_{cat}*[SpoIIAA-P or SpoIIE]/ (K_M^{MnCl2}+ [SpoIIAA-P or SpoIIE]). Reactions with SpoIIAA-P as substrate were performed as multiple-turnover reactions with 0.1

µM SpoIIE, 10 mM $MnCl_2$ and varying concentration of SpoIIAA-P. Reactions with RsbV-P as substrate were performed as single-turnover reactions (necessary due to slow rates of reaction) with 10 mM $MnCl_2$, trace RsbV-P and varying concentrations of SpoIIE. **b.** $SpoIIE^{457-827}$ activity as a function of $MnCl_2$ concentration, with SpoIIAA-P (red) or RsbV-P (blue). Data are fit to a cooperative model using the equation $k_{obs} = k_{cat}*[MnCl_2]^2/ (K_{1/2}+ [MnCl_2]^2)$. Hill plots from the data are shown to the right and are fit to a linear equation. Data for $SpoIIE^{457-827}$ and $SpoIIE^{457-827•V697A}$ with SpoIIAA-P as substrate are from Bradshaw et. al 2017, replotted here for reference. Reactions with RsbV-P as substrate included 50 µM SpoIIE and trace RsbV-P. **c.** A summary of kinetic parameters in the reaction scheme for dephosphorylation by SpoIIE. S indicates the phosphoprotein substrate and P indicates the product.

Figure 4. Mutation of the switch activates RsbU activity in the absence of RsbT. a. RsbU mutants that are active in the absence of RsbT from a blue-white screen using a strain carrying a lacZ-reporter for σ^B activity. Colonies of cells expressing *rsbU*^{M166V} or *rsbU*^{M166L} at the native *rsbU* locus on the chromosome exhibit high levels of σ^B activity both in the presence and absence of *rsbT.* All strains lack *rsbPQ* and carry a reporter for σ^B activity (*amyE::ctc-lacZ*). Strains were grown on LB plates containing 80 µg/ml X-gal at 37ºC and imaged after 18 hours. Presence of blue pigment indicates σ^B activity and activation of the stress response pathway. **b.** A structure of the SpoIIE PP2C domain (PDBID 5UCG), with the cα of V697 and S640 (the equivalent of M166 in RsbU) displayed as green spheres. The α-helical switch is represented in orange and the sidechains that coordinate divalent cations in the active site are shown as sticks. **c.** *rsbU*^{M166L} leads to increased σ^B activity as cultures approach stationary phase. Plots show beta-galactosidase activity from *rsbPQ* deleted strains carrying a lacZ-reporter for σ^B activity (Δ*rsbPQ amyE::ctc*-lacZ) either encoding wild-type *rsbU (*blue), *rsbU*^{M166L} *(*red) (top panel), or deleted for *rsbU (*gray) (bottom panel). Light colors indicate that the strain additionally had *rsbT* deleted (botton panel). The plots show cell-density dependent activation of σ^B from four independent replicates per strain background. Cultures were sampled from early log phase to stationary phase and beta-galactosidase activity is plotted as a function of OD_{600}. *lacZ* expression was analyzed using ONPG as a substrate. NB: Y-axis scales differ between top and bottom panels to allow better visualization of data. **d**. *rsbU*^{M166L} leads to increased responsiveness to ethanol stress. Plots show beta-galactosidase activity from strains described in C. The plots show cell-density dependent activation of σ^B from four independent replicates per strain background. The complete data from each replicate can be viewed in Figure SF2B. Cultures were exposed to 4% ethanol (v/v) at low OD_{600} (~0.1-0.2) to control for cell density-dependent effects on σ^B

activity. Cultures were sampled at early log phase 30 minutes and immediately prior to addition of ethanol and then at regular intervals afterward. *lacZ* activity analyzed as previously described, and mean beta-galactosidase activity is plotted as a function of time of ethanol addition. Error bars reflect standard deviation from the mean. Y-axis scales differ between top and bottom panels to allow better visualization of data.

Figure 5. RsbT modifies RsbU activity and specificity in a manner characteristic of switch-mediated activation. a. Plot of RsbU dephosphorylation of RsbV-P (blue, top) and SpoIIAA-P (red, bottom) in the presence (light color) and absence (dark color) of 10 µM RsbT. Reactions were performed at varying concentrations of $MnCl_2$ and data are fit using nonlinear curve fitting (Kaleidagraph) to the equation $k_{obs} = k_{cat}*[MnCl_2]^h/ (K_{1/2} + [MnCl_2]^h)$. Values of *h* were determined from Hill plots of activity shown to the right (data were fit to a linear equation). For RsbU with RsbV-P *h* is 1.0 (1.0 with T) and 1.4 with SpoIIAA-P (1.6 with T). For reactions with SpoIIAA as substrate, single turnover reactions with 2.5 µM RsbU were performed (due to the slow rates of dephosphorylation). Reactions with RsbV-P as substrate included 25 µM RsbU (single turnover in the absence of T) or 25 µM RsbV-P and 0.5 µM RsbU (multiple turnover in the presence of T because of the rapid rate of dephosphorylation). **b.** Plots of RsbU activity towards RsbV-P (left, blue) and SpoIIAA-P (right, red) in the absence (dark colors) and presence (light colors) of RsbT (10 µM). Curves are fits to the Michaelis-Menton equation rate = $k_{cat}*[\text{RsbU or RsbV-P}]/ (K_M+ [\text{RsbU or RsbV-P}])$. The k_{cat} for RsbV-P is 25 min^{-1} (0.4 min^{-1} without T) and K_M 1.3 µM (1.5 µM without T). The k_{cat} for SpoIIAA-P is 0.32 min^{-1} (0.0012 min^{-1} without T) and K_M 0.3 µM (1 µM without T). Multiple turnover reactions included 0.1 µM RsbU and all reactions were performed with saturating $MnCl_2$ (100 mM except for 10 mM for

reactions of RsbV-P in the presence of T). **c.** A summary of the reaction scheme for RsbU dephosphorylation with values determined for $K_{1/2}$ for $MnCl_2$, K_M for substrate, and k_{cat} in the presence and absence of RsbT below. S indicates the phosphoprotein substrate and P indicates the product.

References:

1. Huse, M., and Kuriyan, J. (2002) The conformational plasticity of protein kinases. *Cell*. **109**, 275–282
2. Taylor, S. S., and Kornev, A. P. (2011) Protein kinases: evolution of dynamic regulatory proteins. *Trends Biochem. Sci.* **36**, 65–77
3. Ubersax, J. A., and Ferrell, J. E. (2007) Mechanisms of specificity in protein phosphorylation. *Nat. Rev. Mol. Cell Biol.* **8**, 530–541
4. Shi, Y. (2009) Serine/threonine phosphatases: mechanism through structure. *Cell*. **139**, 468–484
5. Moorhead, G. B. G., De Wever, V., Templeton, G., and Kerk, D. (2009) Evolution of protein phosphatases in plants and animals. *Biochem J*. **417**, 401–409
6. Kerk, D., Silver, D., Uhrig, R. G., and Moorhead, G. B. G. (2015) "PP2C7s," Genes Most Highly Elaborated in Photosynthetic Organisms, Reveal the Bacterial Origin and Stepwise Evolution of PPM/PP2C Protein Phosphatases. *PLoS ONE*. **10**, e0132863
7. Lammers, T., and Lavi, S. (2007) Role of type 2C protein phosphatases in growth regulation and in cellular stress signaling. *Crit Rev Biochem Mol Biol*. **42**, 437–461
8. Stragier, P., and Losick, R. (1996) Molecular genetics of sporulation in Bacillus subtilis. *Annu Rev Genet*. **30**, 297–241
9. Bradshaw, N., and Losick, R. (2015) Asymmetric division triggers cell-specific gene expression through coupled capture and stabilization of a phosphatase. *eLife*. 10.7554/eLife.08145
10. Duncan, L., Alper, S., Arigoni, F., Losick, R., and Stragier, P. (1995) Activation of cell-specific transcription by a serine phosphatase at the site of asymmetric division. *Science*. **270**, 641–644
11. Bradshaw, N., Levdikov, V. M., Zimanyi, C. M., Gaudet, R., Wilkinson, A. J., and Losick, R. (2017) A widespread family of serine/threonine protein phosphatases shares a common regulatory switch with proteasomal proteases. *eLife*. 10.7554/eLife.26111
12. Yang, X., Kang, C. M., Brody, M. S., and Price, C. W. (1996) Opposing pairs of serine protein kinases and phosphatases transmit signals of environmental stress to activate a bacterial transcription factor. *Genes Dev*. **10**, 2265–2275
13. Gottesman, S. (2019) Trouble is coming: Signaling pathways that regulate general stress responses in bacteria. 10.1074/jbc.REV119.005593
14. Carniol, K., Kim, T.-J., Price, C. W., and Losick, R. (2004) Insulation of the sigmaF regulatory system in Bacillus subtilis. *J Bacteriol*. **186**, 4390–4394
15. Rothstein, D. M., Lazinski, D., Osburne, M. S., and Sonenshein, A. L. (2017) A Mutation in the Bacillus subtilis rsbU Gene That Limits RNA Synthesis during Sporulation. *J Bacteriol*. 10.1128/JB.00212-17
16. Cabeen, M. T., Russell, J. R., Paulsson, J., and Losick, R. (2017) Use of a microfluidic platform to uncover basic features of energy and environmental stress responses in individual cells of Bacillus subtilis. *PLoS Genet*. **13**, e1006901
17. Locke, J. C. W., Young, J. W., Fontes, M., Jimenez, M. J. H., and Elowitz, M. B. (2011) Stochastic Pulse Regulation in Bacterial Stress Response. *Science*. **334**, 366–369
18. Carniol, K., Eichenberger, P., and Losick, R. (2004) A threshold mechanism governing activation of the developmental regulatory protein sigma F in Bacillus subtilis. **279**, 14860–14870

19. Hilbert, D. W., and Piggot, P. J. (2003) Novel spoIIE mutation that causes uncompartmentalized sigmaF activation in Bacillus subtilis. *J Bacteriol*. **185**, 1590–1598
20. Delumeau, O., Dutta, S., Brigulla, M., Kuhnke, G., Hardwick, S. W., Völker, U., Yudkin, M. D., and Lewis, R. J. (2004) Functional and structural characterization of RsbU, a stress signaling protein phosphatase 2C. **279**, 40927–40937
21. Scribner, H., Eisenstadt, E., and Silver, S. (1974) Magnesium transport in Bacillus subtilis W23 during growth and sporulation. *J Bacteriol*. **117**, 1224–1230
22. Eisenstadt, E., Fisher, S., Der, C. L., and Silver, S. (1973) Manganese transport in Bacillus subtilis W23 during growth and sporulation. *J Bacteriol*. **113**, 1363–1372
23. Soon, F.-F., Ng, L.-M., Zhou, X. E., West, G. M., Kovach, A., Tan, M. H. E., Suino-Powell, K. M., He, Y., Xu, Y., Chalmers, M. J., Brunzelle, J. S., Zhang, H., Yang, H., Jiang, H., Li, J., Yong, E.-L., Cutler, S., Zhu, J.-K., Griffin, P. R., Melcher, K., and Xu, H. E. (2012) Molecular mimicry regulates ABA signaling by SnRK2 kinases and PP2C phosphatases. *Science*. **335**, 85–88
24. Poh, W.-H., Lin, J., Colley, B., Müller, N., Goh, B. C., Schleheck, D., Sahili, El, A., Marquardt, A., Liang, Y., Kjelleberg, S., Lescar, J., Rice, S. A., and Klebensberger, J. (2020) The SiaABC threonine phosphorylation pathway controls biofilm formation in response to carbon availability in Pseudomonas aeruginosa. *PLoS ONE*. **15**, e0241019
25. Levchenko, I., Grant, R. A., Sauer, R. T., and Baker, T. A. (2009) Structure of Orthorhombic crystal form of Pseudomonas aeruginosa RssB. 10.2210/pdb3f7a/pdb
26. Zhang, Y., Zhao, H., Wang, J., Ge, J., Li, Y., Gu, J., Li, P., Feng, Y., and Yang, M. (2013) Structural insight into Caenorhabditis elegans sex-determining protein FEM-2. **288**, 22058–22066
27. Vassylyev, D. G., and Symersky, J. (2007) Crystal structure of pyruvate dehydrogenase phosphatase 1 and its functional implications. *J Mol Biol*. **370**, 417–426
28. Dorich, V., Brugger, C., Tripathi, A., Hoskins, J. R., Tong, S., Suhanovsky, M. M., Sastry, A., Wickner, S., Gottesman, S., and Deaconescu, A. M. (2019) Structural basis for inhibition of a response regulator of σS stability by a ClpXP antiadaptor. *Genes Dev*. **33**, 718–732
29. Mazur, S. J., Gallagher, E. S., Debnath, S., Durell, S. R., Anderson, K. W., Miller Jenkins, L. M., Appella, E., and Hudgens, J. W. (2017) Conformational Changes in Active and Inactive States of Human PP2Cα Characterized by Hydrogen/Deuterium Exchange-Mass Spectrometry. *Biochemistry*. **56**, 2676–2689
30. Vintonyak, V. V., Waldmann, H., and Rauh, D. (2011) Using small molecules to target protein phosphatases. *Bioorg. Med. Chem.* **19**, 2145–2155
31. Carrara, M., Sigurdardottir, A., and Bertolotti, A. (2017) Decoding the selectivity of eIF2α holophosphatases and PPP1R15A inhibitors. *Nature Structural & Molecular Biology*. **24**, 708–716
32. Morita, K., He, S., Nowak, R. P., Wang, J., Zimmerman, M. W., Fu, C., Durbin, A. D., Martel, M. W., Prutsch, N., Gray, N. S., Fischer, E. S., and Look, A. T. (2020) Allosteric Activators of Protein Phosphatase 2A Display Broad Antitumor Activity Mediated by Dephosphorylation of MYBL2. *Cell*. **181**, 702–715.e20
33. Pádua, R. A. P., Sun, Y., Marko, I., Pitsawong, W., Stiller, J. B., Otten, R., and Kern, D. (2018) Mechanism of activating mutations and allosteric drug inhibition of the phosphatase SHP2. *Nat Commun*. **9**, 4507–14

34. Gilmartin, A. G., Faitg, T. H., Richter, M., Groy, A., Seefeld, M. A., Darcy, M. G., Peng, X., Federowicz, K., Yang, J., Zhang, S.-Y., Minthorn, E., Jaworski, J.-P., Schaber, M., Martens, S., McNulty, D. E., Sinnamon, R. H., Zhang, H., Kirkpatrick, R. B., Nevins, N., Cui, G., Pietrak, B., Diaz, E., Jones, A., Brandt, M., Schwartz, B., Heerding, D. A., and Kumar, R. (2014) Allosteric Wip1 phosphatase inhibition through flap-subdomain interaction. *Nat Chem Biol*. **10**, 181–187
35. Tagad, H. D., Debnath, S., Clausse, V., Saha, M., Mazur, S., Appella, E., and Appella, D. H. (2018) Chemical features important for activity in a class of inhibitors targeting the Wip1 flap subdomain. *ChemMedChem*. 10.1002/cmdc.201700779
36. Levdikov, V. M., Blagova, E. V., Rawlings, A. E., Jameson, K., Tunaley, J., Hart, D. J., Barak, I., and Wilkinson, A. J. (2012) Structure of the phosphatase domain of the cell fate determinant SpoIIE from Bacillus subtilis. *J Mol Biol*. **415**, 343–358
37. Harwood, C. R., and Cutting, S. M. (2010) Molecular Biological Methods for Bacillus
38. Youngman, P., Perkins, J. B., and Losick, R. (1984) Construction of a cloning site near one end of Tn917 into which foreign DNA may be inserted without affecting transposition in Bacillus subtilis or expression of the transposon-borne erm gene. *Plasmid*. **12**, 1–9
39. Zeigler, D. R., Prágai, Z., Rodriguez, S., Chevreux, B., Muffler, A., Albert, T., Bai, R., Wyss, M., and Perkins, J. B. (2008) The origins of 168, W23, and other Bacillus subtilis legacy strains. *J Bacteriol*. **190**, 6983–6995
40. Arnaud, M., Chastanet, A., and Debarbouille, M. (2004) New vector for efficient allelic replacement in naturally nontransformable, low-GC-content, gram-positive bacteria. *Applied and Environmental Microbiology*. **70**, 6887–6891
41. Carniol, K., Ben-Yehuda, S., King, N., and Losick, R. (2005) Genetic dissection of the sporulation protein SpoIIE and its role in asymmetric division in Bacillus subtilis. *J Bacteriol*. **187**, 3511–3520
42. Bron, S., Bolhuis, A., Tjalsma, H., Holsappel, S., Venema, G., and van Dijl, J. M. (1998) Protein secretion and possible roles for multiple signal peptidases for precursor processing in bacilli. *J Biotechnol*. **64**, 3–13
43. The PyMOL Molecular Graphics System, Version 2.0 Schrödinger, LLC.
44. UCSF Chimera--a visualization system for exploratory research and analysis. Pettersen EF, Goddard TD, Huang CC, Couch GS, Greenblatt DM, Meng EC, Ferrin TE. *J Comput Chem.* 2004 Oct;25(13):1605-12.

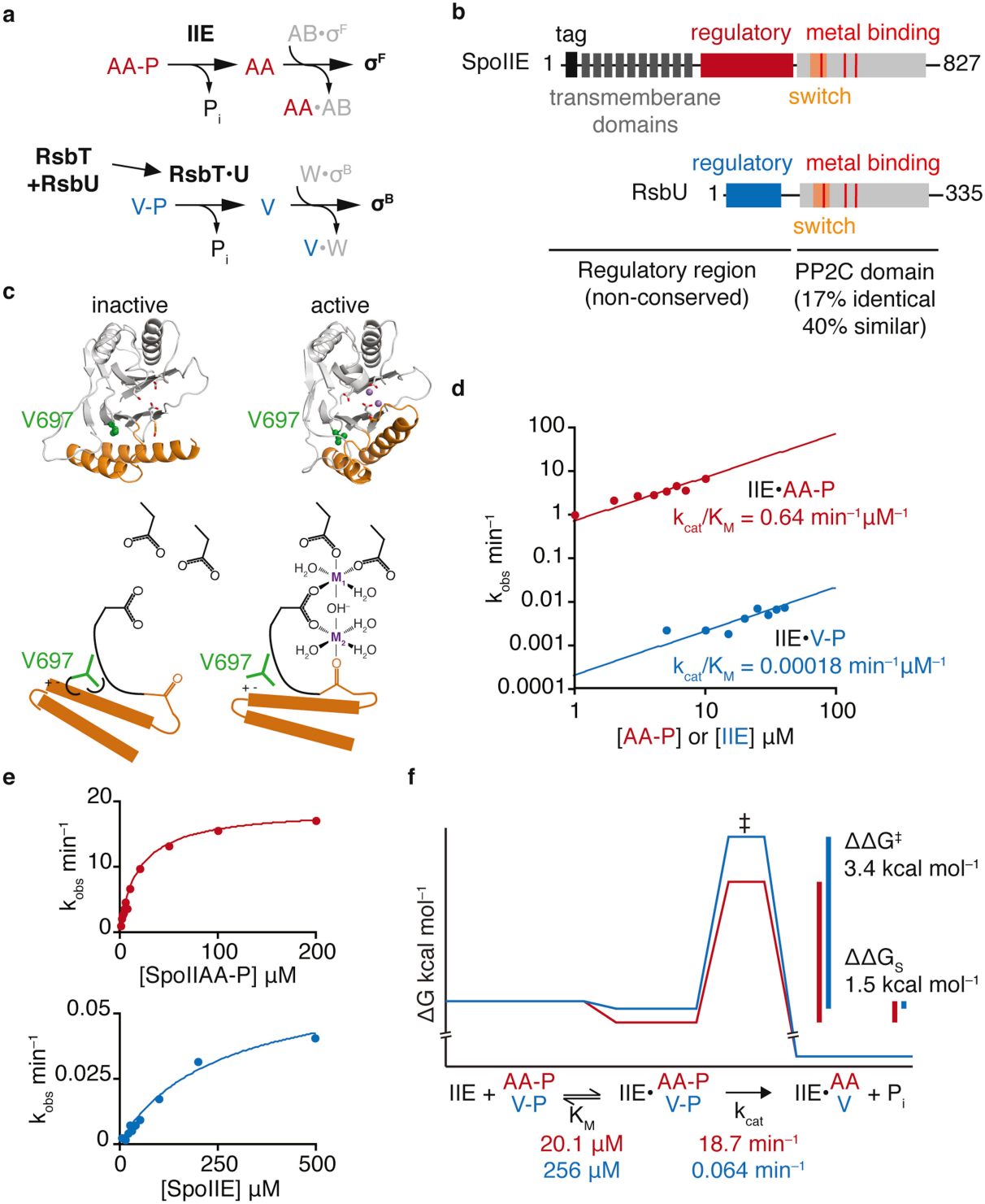
a
IIE
AA-P
AA
P i
AB•σF
σF
AA•AB
RsbT
+RsbU
RsbT•U
V-P
V
P i
W•σB
σB
V•W
b
tag
regulatory
metal binding
SpoIIE
1
827
transmemberane
domains
switch
regulatory
metal binding
RsbU
1
335
switch
Regulatory region
(non-conserved)
PP2C domain
(17% identical
40% similar)
c
inactive
active
V697
V697
V697
V697
d
IIE•AA-P
kcat/KM = 0.64 min−1μM−1
IIE•V-P
kcat/KM = 0.00018 min−1μM−1
kobs min−1
[AA-P] or [IIE] μM
e
kobs min−1
[SpoIIAA-P] μM
kobs min−1
[SpoIIE] μM
f
ΔG kcal mol−1
ΔΔG‡
3.4 kcal mol−1
ΔΔGS
1.5 kcal mol−1
IIE + AA-P / V-P
KM
IIE• AA-P / V-P
kcat
IIE• AA / V + Pi
20.1 μM
256 μM
18.7 min−1
0.064 min−1

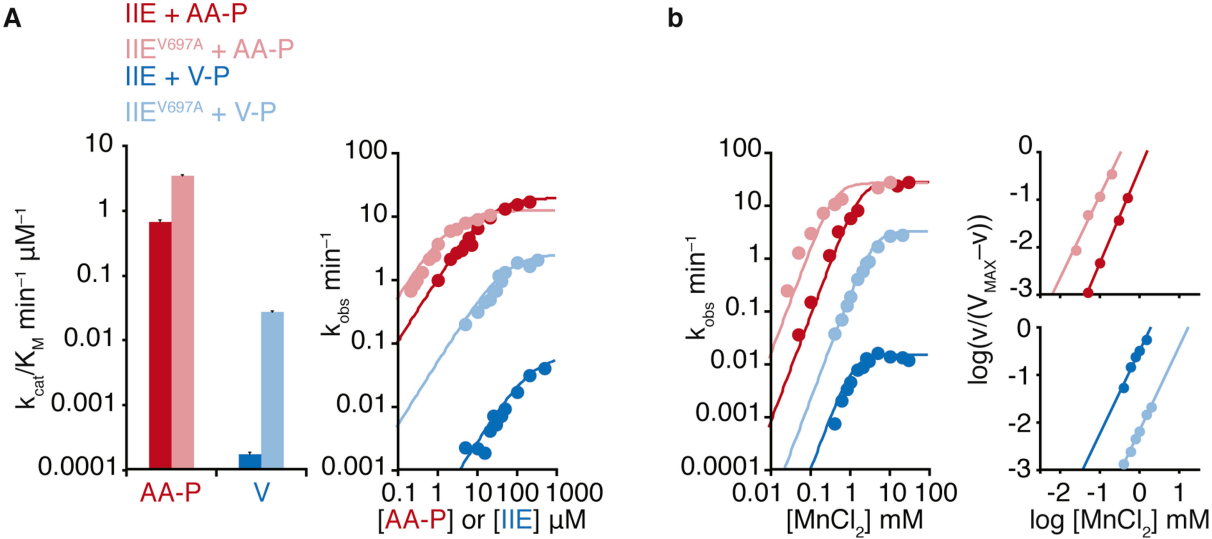

c

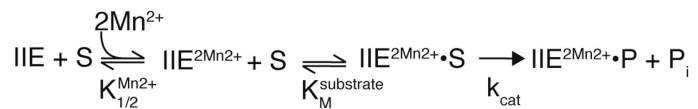

AA-P:	3.1(0.16) mM	20(2.4) μM	19(12) min^{-1}
V-P:	2.0(19) mM	256(55) μM	0.064(2.4) min^{-1}

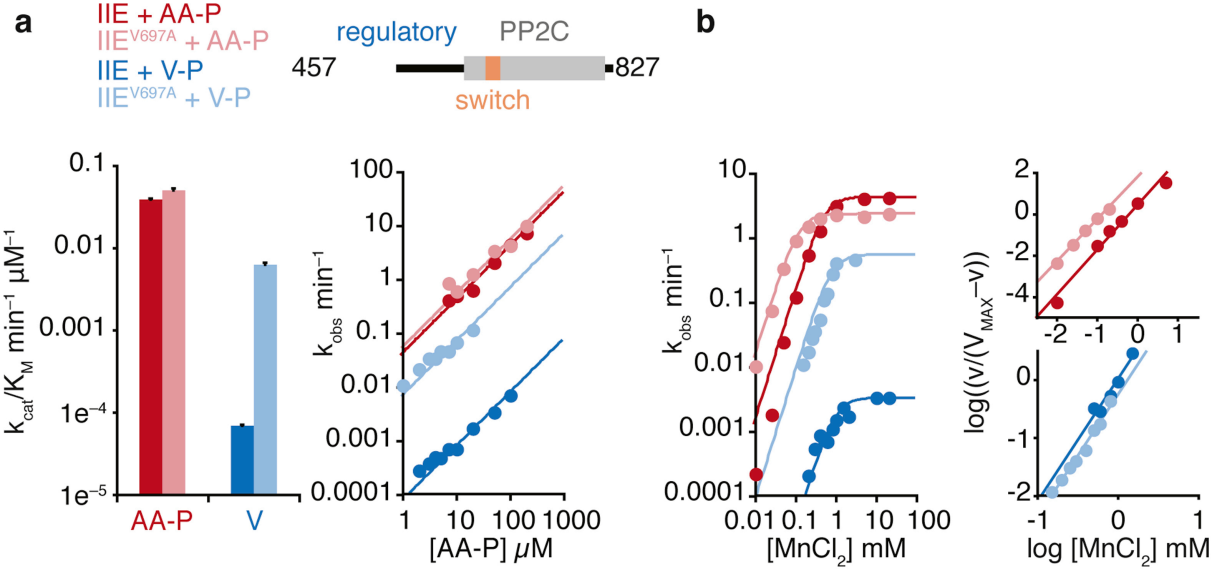
a
IIE + AA-P
IIE^V697A + AA-P
IIE + V-P
IIE^V697A + V-P
regulatory
PP2C
457
827
switch
b
0.1
0.01
0.001
1e−4
1e−5
kcat/KM min−1 μM−1
AA-P
V
100
10
1
0.1
0.01
0.001
0.0001
kobs min−1
1
10
100
1000
[AA-P] μM
10
1
0.1
0.01
0.001
0.0001
kobs min−1
0.01
0.1
1
10
100
[MnCl2] mM
2
0
-2
-4
-2
-1
0
1
0
-1
-2
-1
0
1
log((v/(VMAX−v))
log [MnCl2] mM
c
2Mn2+
IIE + S
IIE2Mn2+ + S
IIE2Mn2+•P + Pi
K1/2 Mn2+
kcat/KM
AA-P: 0.32(0.017) mM 0.039(0.050) μM−1min−1
V-P: 1.1(0.69) mM 7.2e−5(0.0064) μM−1min−1

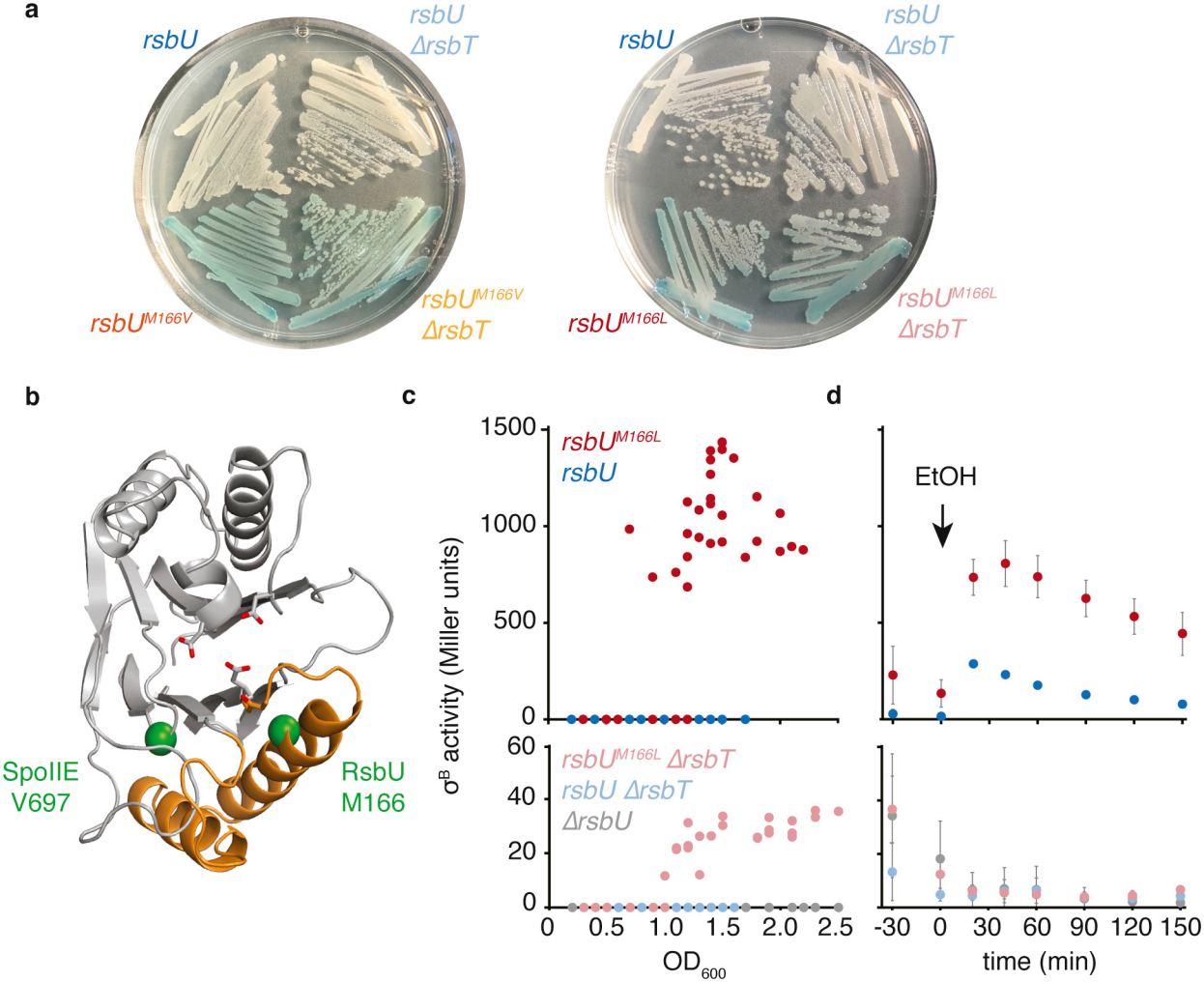
a
rsbU
rsbU ΔrsbT
rsbU^M166V
rsbU^M166V ΔrsbT
rsbU
rsbU ΔrsbT
rsbU^M166L
rsbU^M166L ΔrsbT
b
SpoIIE V697
RsbU M166
c
rsbU^M166L
rsbU
rsbU^M166L ΔrsbT
rsbU ΔrsbT
ΔrsbU
σB activity (Miller units)
1500
1000
500
0
60
40
20
0
0
0.5
1.0
1.5
2.0
2.5
OD600
d
EtOH
-30
0
30
60
90
120
150
time (min)

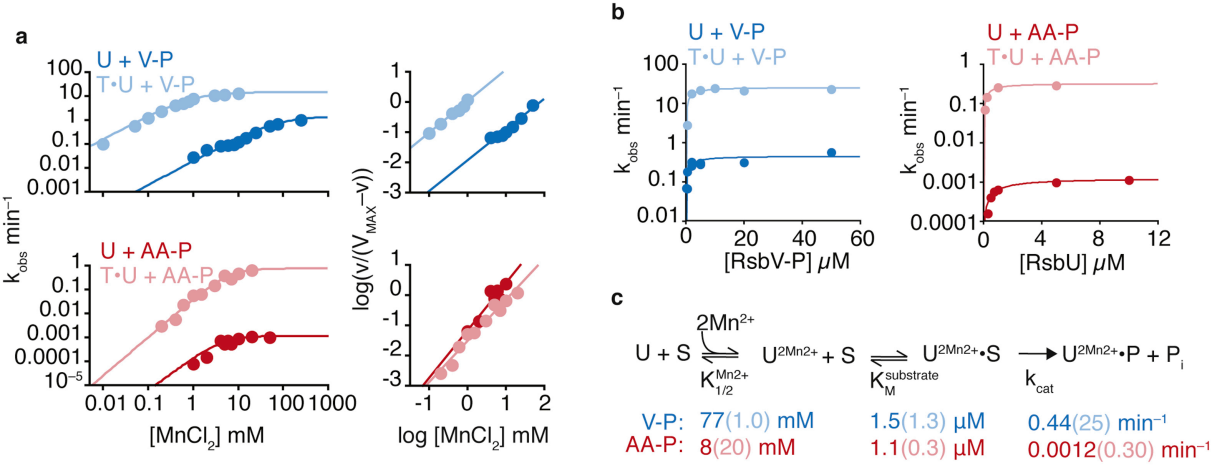
a
U + V-P
T•U + V-P
U + AA-P
T•U + AA-P
k_{obs} min^{-1}
[MnCl$_2$] mM
log(v/(V$_{MAX}$−v))
log [MnCl$_2$] mM
b
U + V-P
T•U + V-P
U + AA-P
T•U + AA-P
k_{obs} min^{-1}
[RsbV-P] μM
[RsbU] μM
c
$2Mn^{2+}$
$U + S \rightleftharpoons U^{2Mn2+} + S \rightleftharpoons U^{2Mn2+}{\bullet}S \rightarrow U^{2Mn2+}{\bullet}P + P_i$
$K_{1/2}^{Mn2+}$
$K_M^{substrate}$
k_{cat}
V-P: 77(1.0) mM 1.5(1.3) μM 0.44(25) min^{-1}
AA-P: 8(20) mM 1.1(0.3) μM 0.0012(0.30) min^{-1}